

Strengthening of the Pacific Equatorial Undercurrent in the SODA Reanalysis: Mechanisms, Ocean Dynamics, and Implications

ELIZABETH J. DRENKARD

*Massachusetts Institute of Technology/Woods Hole Oceanographic Institution Joint Program in Oceanography,
Cambridge, Massachusetts*

KRISTOPHER B. KARNAUSKAS

Woods Hole Oceanographic Institution, Woods Hole, Massachusetts

(Manuscript received 21 June 2013, in final form 6 December 2013)

ABSTRACT

Several recent studies utilizing global climate models predict that the Pacific Equatorial Undercurrent (EUC) will strengthen over the twenty-first century. Here, historical changes in the tropical Pacific are investigated using the Simple Ocean Data Assimilation (SODA) reanalysis toward understanding the dynamics and mechanisms that may dictate such a change. Although SODA does not assimilate velocity observations, the seasonal-to-interannual variability of the EUC estimated by SODA corresponds well with moored observations over a ~ 20 -yr common period. Long-term trends in SODA indicate that the EUC core velocity has increased by 16% century⁻¹ and as much as 47% century⁻¹ at fixed locations since the mid-1800s. Diagnosis of the zonal momentum budget in the equatorial Pacific reveals two distinct seasonal mechanisms that explain the EUC strengthening. The first is characterized by strengthening of the western Pacific trade winds and hence oceanic zonal pressure gradient during boreal spring. The second entails weakening of eastern Pacific trade winds during boreal summer, which weakens the surface current and reduces EUC deceleration through vertical friction. EUC strengthening has important ecological implications as upwelling affects the thermal and biogeochemical environment. Furthermore, given the potential large-scale influence of EUC strength and depth on the heat budget in the eastern Pacific, the seasonal strengthening of the EUC may help reconcile paradoxical observations of Walker circulation slowdown and zonal SST gradient strengthening. Such a process would represent a new dynamical “thermostat” on CO₂-forced warming of the tropical Pacific Ocean, emphasizing the importance of ocean dynamics and seasonality in understanding climate change projections.

1. Introduction

The Equatorial Undercurrent (EUC) is the swiftest, most coherent eastward-moving flow in the tropical Pacific Ocean (e.g., Philander 1973; Wyrtki and Kilonsky 1984; Philander et al. 1987). The EUC slopes upward from 200 ± 100 m at 156°E to 100 ± 100 m at 95°W and is confined to within $\sim 2^\circ$ latitude of the equator (summarized in Arthur 1960; Johnson et al. 2002). The zonal pressure gradient force, related to the zonal sea level slope, is maintained by the easterly trade winds and the westward surface current and constitutes a dominant acceleration term in the momentum budget of the EUC

(Knauss 1960, 1966). The balance between the eastward zonal pressure gradient force and westward surface stress determines the strength as well as zonal and vertical structure of the EUC (Philander 1973; McPhaden and Taft 1988).

The EUC plays a crucial role in Pacific and global climate processes and biogeochemical cycles; it delivers cold, CO₂- and nutrient-rich water to the eastern Pacific, where it feeds the cold tongue. Here, EUC water contributes to the largest oceanic source of atmospheric CO₂ (e.g., Feely et al. 2006) and to maintaining the zonal sea surface temperature (SST) gradient across the Pacific (Bjerknes 1966). This thermal gradient is one of the primary controls on tropical Pacific atmospheric circulation, which affects weather patterns and climate worldwide (e.g., Bjerknes 1969; Julian and Chervin 1978). Additionally, upwelling of EUC water provides

Corresponding author address: Liz Drenkard, 266 Woods Hole Rd., MS 23, Woods Hole, MA 02543-1050.
E-mail: edrenkard@whoi.edu

thermal balance and nutrients to valuable fisheries (e.g., Ganachaud et al. 2012) and equatorial island ecosystems (e.g., Houvenaghel 1978; Gove et al. 2006; Karnauskas and Cohen 2012). Therefore, changes in EUC intensity will likely have important climatic and ecological repercussions.

Studies predicting future EUC strengthening (e.g., Luo et al. 2009; Karnauskas and Cohen 2012; Sen Gupta et al. 2012) have attributed this change to rising concentrations of atmospheric CO₂. Anthropogenic CO₂ emissions have unequivocally affected atmospheric composition over the past century (Mann et al. 1999; Keeling et al. 1976). Thus it begs the question: Has the EUC already responded to historical CO₂ forcing? If so, is it consistent with the future change predicted by global coupled models, is it significant, and can it be explained in a robust dynamical framework? In this study, we used the most recent version of a widely accepted ocean data assimilation product to analyze past trends in EUC strength and to diagnose the oceanic and atmospheric mechanisms driving these changes. The following sections describe the reanalysis dataset we analyzed and methods we followed to determine the historical trends and evaluate the equatorial Pacific zonal momentum budget. The results of these analyses are reported in section 3 and discussed within the context of their potential climatological and ecological significance in section 4.

2. Data

We analyzed the most recent version of the Simple Ocean Data Assimilation (SODA) reanalysis (version 2.2.6; Yang and Giese 2013) to characterize and understand historical changes in EUC strength. This version of SODA and its predecessors (Carton and Giese 2008) are data assimilation products: ocean general circulation models constrained by quality-controlled observations. Monthly SODA fields extend from 1871 to 2008 and are the ensemble mean of eight model runs, each driven by a different realization of wind stress and variables needed for the calculation of heat and freshwater fluxes from the National Oceanic and Atmospheric Administration (NOAA) twentieth-century atmospheric reanalysis (Compo et al. 2011; Yang and Giese 2013), thus ensuring that the statistics of weather noise do not change over time. Furthermore, version 2.2.6 assimilates observations of SST only, which prevents the appearance of spurious trends and shifts due to the rise of hydrographic measurements starting in the late 1960s. The spatial and temporal completeness of SODA allows for rigorous assessment of EUC structure and dynamics over long periods of time; such assessments are not typically possible with in situ

observations alone. Throughout this paper, we frequently refer to “observed” phenomena; it should be understood that we are referring to results derived from the SODA reanalysis.

The sources of observational data assimilated vary by reanalysis product and even by version within families of reanalyses, but in no case are in situ ocean subsurface velocities assimilated. Figure 1 compares acoustic Doppler current profiler (ADCP) measurements of the EUC from equatorial Tropical Atmosphere Ocean (TAO; McPhaden et al. 1998) moorings with coinciding SODA estimates. We include comparison of both monthly (Figs. 1a,c,e,g) and normalized filtered (13-month running mean) time series (Figs. 1b,d,f,h) to assess correspondence between reanalysis and TAO variability at both annual and lower than annual frequencies. With the exception of 0°, 170°W, where there is not a significant difference between SODA and TAO records (Table 1), the SODA reanalysis tends to underestimate the EUC’s maximum zonal velocity by ~10 cm s⁻¹; this may be related to the reanalysis’s relatively coarse spatial resolution (Karnauskas et al. 2012). However, as evidenced by the correlation coefficients for each comparison (reported in Table 1) and similar comparisons in the literature (Seidel and Giese 1999), SODA captures the seasonal-to-interannual variability of the EUC quite well.

3. Results

a. Observed trends in the EUC and other basin-scale fields

The linear trends in the short, coinciding SODA and TAO time series are also reported in Table 1. With the exception of the filtered time series at 165°E (where proximity to land/basin edge may complicate modeled ocean dynamics), none of the SODA trends at a given longitude and smoothing regime differ significantly from their TAO counterparts. Additionally, the majority of these trends are positive and, particularly among the filtered time series, significantly greater than zero.

We first investigated the trends in annual-mean zonal velocity at a fixed point within the mean-state core of the EUC (0°, 146°W, 112-m depth; Fig. 2). Here we observe a trend of $0.43 \pm 0.10 \text{ m s}^{-1}$ per century (equivalent to 47% century⁻¹ of the annual mean) increase in zonal velocity since 1871. However, the position and structure of the EUC are not fixed in time (e.g., Philander 1973; Johnson et al. 2002) and, therefore, evaluating temporal trends in zonal velocity at a single depth and geographic location could potentially exaggerate or underrepresent comprehensive changes in the undercurrent. To account for this, we compiled and evaluated a monthly time

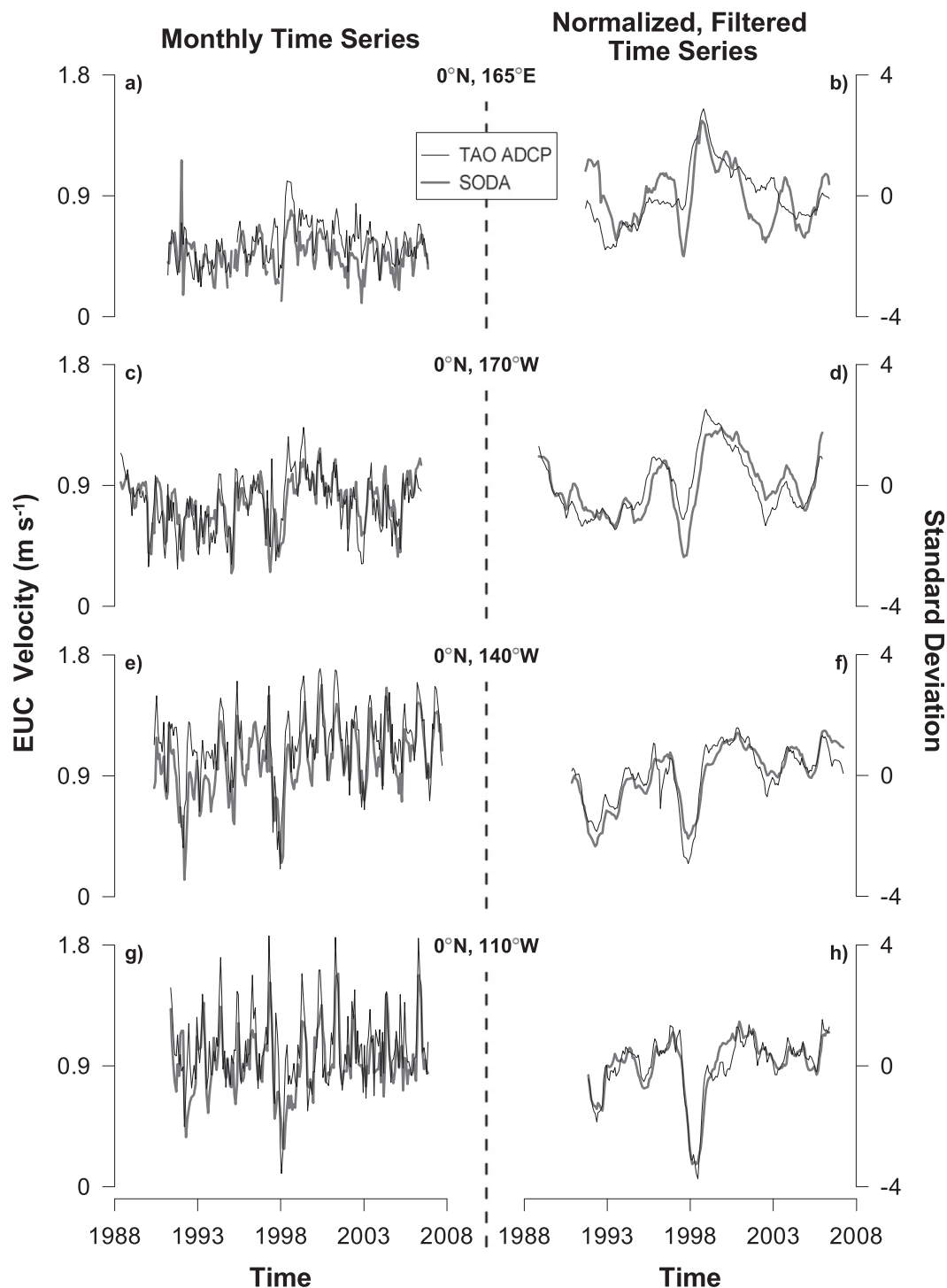


FIG. 1. Comparison of max EUC zonal velocity estimated by SODA (gray) and ADCP measurements by equatorial TAO moorings (black) at 0° lat and (a),(b) 165°E ; (c),(d) 170°W ; (e),(f) 140°W ; and (g),(h) 110°W . The ADCP data were regridded via linear interpolation to depth intervals that match the vertical resolution of SODA; max velocities located below 300 m were masked out. The monthly time series of max zonal velocity are compared in (a),(c),(e),(g); while these time series after filtering (13-month running mean) and normalization are compared in (b),(d),(f),(h).

TABLE 1. Correlation coefficients R , average SODA–ADCP bias, and linear trends for both monthly and filtered time series. All correlation and bias values (with the exception of biases reported at 170°W) are significant ($\alpha = 0.01$; $p < 0.001$).

		Equatorial TAO locations (lon)			
		165°E	170°W	140°W	110°W
Monthly time series	R	0.53	0.75	0.82	0.75
	Bias (m s^{-1})	-0.08	0.01	-0.14	-0.10
	ADCP trend ($\text{m s}^{-1} \text{ century}^{-1}$)	0.61 ± 0.63	0.44 ± 0.71	$1.15 \pm 0.94^*$	0.61 ± 1.18
	SODA trend ($\text{m s}^{-1} \text{ century}^{-1}$)	-0.16 ± 0.58	$0.71 \pm 0.62^*$	$2.10 \pm 0.83^*$	0.82 ± 1.01
Monthly time series (13-month smoothing filter)	R	0.60	0.84	0.91	0.93
	Bias (m s^{-1})	-0.09	0.01	-0.14	-0.10
	ADCP trend ($\text{m s}^{-1} \text{ century}^{-1}$)	$0.70 \pm 0.44^*$	$0.64 \pm 0.47^*$	$1.31 \pm 0.43^*$	$0.70 \pm 0.39^*$
	SODA trend ($\text{m s}^{-1} \text{ century}^{-1}$)	-0.17 ± 0.31	$0.73 \pm 0.40^*$	$2.20 \pm 0.44^*$	$0.91 \pm 0.51^*$

* Statistically significant trend ($\alpha = 0.01$).

series (Fig. 2) of the maximum zonal velocity found in the spatial domain: 2°N–2°S, 150°–90°W and 10–300-m depth. This time series effectively tracks the velocity at the center of the EUC core over the course of the SODA record. The $0.17 \pm 0.03 \text{ m s}^{-1} \text{ century}^{-1}$ trend in maximum zonal velocity indicates that the core of the EUC has sped up significantly over 1871–2008 (Fig. 2). This observed trend, equivalent to roughly 16% of the twentieth-century mean, is in excellent agreement with the 14.4% EUC strengthening that phase 3 of the Coupled Model Intercomparison Project (CMIP3)/International Panel on Climate Change Fourth Assessment Report (IPCC AR4) global climate models predict for the twenty-first century in response to increasing atmospheric greenhouse gases (Karnauskas and Cohen 2012).

To analyze large-scale trends in EUC velocity including their spatial variation, we repeated the analysis for Fig. 2 at 0°, 146°W, and 112-m depth for all depths and longitudes along the equator. With this, we produced a depth–longitude cross section showing the long-term trends in zonal velocity (colored contours in Fig. 3a) set in the context of the mean-state zonal velocity (black contours in Fig. 3a). Because the EUC flows along the pycnocline and is sensitive to stratification (Philander 1973), we also include a complementary depth profile (Fig. 3b) of the vertical density gradient in order to provide additional context for the structural changes we observe in the EUC.

The longitude versus depth section of the observed trends in zonal velocity (Fig. 3a) illustrates the structure and nature of the observed strengthening which entails a westward translation and shoaling of the time-mean EUC core and weakening of the South Equatorial Current (SEC). The observation that the region below the EUC core also exhibits a significant trend toward a stronger,

eastward velocity confirms that this is not simply a long-term translation but a significant intensification of the EUC. In the density gradient profile, the stratification increase and reduction that occurs above and below the thermocline, respectively, indicates a shoaling of the mean-state thermocline, west of 130°W (Fig. 3b). However, the regions of maximum gradient intensification and weakening do not occur at the same longitude. East of 150°W, the shallower increase in stratification exceeds the magnitude of the deeper decrease in stratification, which suggests a sharpening of the thermocline similar to the findings of DiNezio et al. (2009). The opposite is found between 170°E and 150°W, indicating a diffusing of the thermocline that spatially corresponds with the region of maximum EUC strengthening (Fig. 3a).

We turn now toward potential dynamical mechanisms for the observed EUC intensification. Here, we consider the long-term trends in maximum EUC velocity in relation to potential drivers for these trends. We compared, by longitude, the trends in zonal wind stress, surface zonal velocity, and maximum zonal velocity (depth range: 10–300 m) on the equator (Figs. 4a–c, respectively). Maximum zonal velocity trends (Fig. 4c) indicate a significant, nearly basinwide strengthening of the EUC in excess of $0.25 \text{ m s}^{-1} \text{ century}^{-1}$ at 150°W. The majority of EUC strengthening (i.e., above $0.1 \text{ m s}^{-1} \text{ century}^{-1}$) is accompanied by significant slowing of the westward surface current between longitudes 180° and 115°W (Fig. 4b). This speaks to the mechanism speculated upon by Karnauskas and Cohen (2012) wherein a reduction in the friction or downward mixing of westward momentum imposed by the surface current would cause the EUC to locally accelerate. However, the long-term trend in zonal wind stress as a function of longitude (Fig. 4a) is at apparent odds with this mechanism: maximum EUC strengthening at 150°W does not coincide

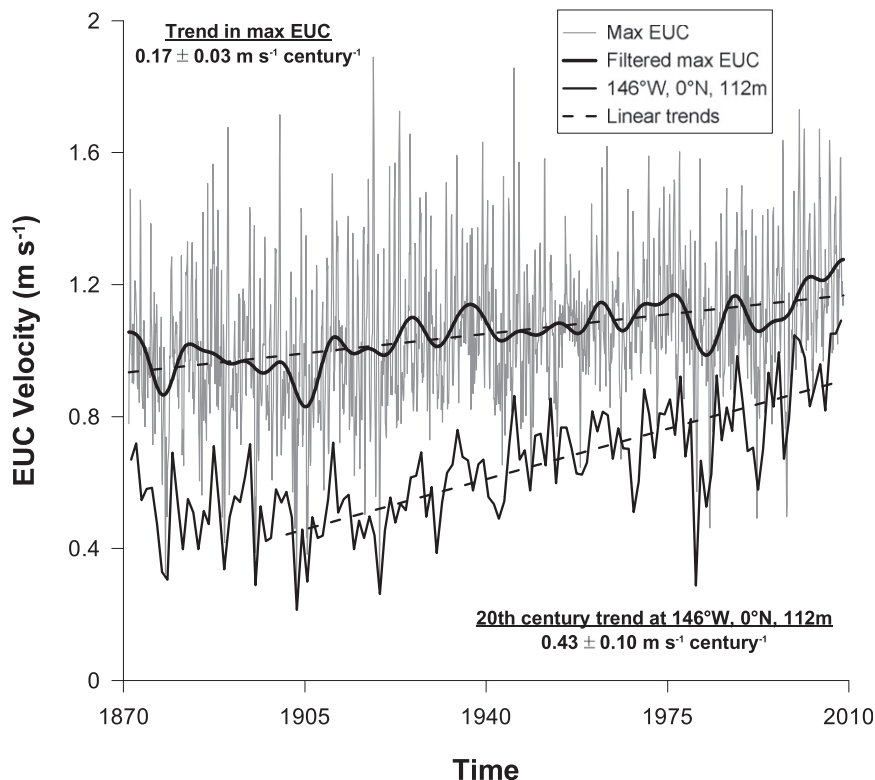


FIG. 2. Time series of max EUC strength and zonal velocity at 0° , 146°W and 112-m depth. The solid, pale gray line depicts the monthly max velocity from SODA within the domain of the EUC core (i.e., 2°N – 2°S , 150° – 90°W ; depth: 10–300 m), while the thick black line is a 7-yr filtering of this time series. The solid, dark gray line indicates the annual-mean zonal velocity at the fixed location: 0° , 146°W and 112-m depth. Finally, we report two linear trends (i.e., regression slopes; dashed lines) for the annual and monthly time series, which are both significant at the 99% confidence interval.

with the point of maximum wind stress weakening ($\sim 105^{\circ}\text{W}$). Two observations in particular prompted the remainder of our efforts to diagnose EUC intensification: The nonuniformity in zonal wind stress trends across the basin (i.e., weakening in the east versus strengthening in the west) likely affects the longitudinal gradient in sea surface height, which suggests that forces such as the zonal pressure gradient may also influence the observed trends in EUC strength. Additionally, the trends shown in Figs. 2–4 are annual-mean perspectives; if the dynamics driving EUC acceleration are seasonally dependent, averaging over the annual cycle may obscure specific mechanisms.

Therefore, we also considered seasonal trends in zonal wind stress, surface ocean velocity, sea surface height, zonal transport, and maximum zonal velocity (colored contours in Figs. 5a–e, respectively). Each field is shown in the context of its climatology (black contours in Figs. 5a–e). We used a depth range of 0–640 m (first 20 depth layers in SODA reanalysis) to calculate zonal transport, a depth range of 10–300 m to determine maximum zonal

velocity, and a horizontal dimension of 110.6 km between latitudes for calculating transport between 0.5°N and 0.5°S . Climatological Hovmöller diagrams (longitude versus time; Fig. 5) highlight two seasons within the annual cycle that clearly dominate the observed EUC intensification. These periods are March–May (MAM) and June–August (JJA); they are characterized by the largest positive trends in eastward volume transport (Fig. 5d) and maximum zonal velocity (Fig. 5e). The MAM intensification occurs approximately one month after maximum strengthening of the easterly trades and westward surface velocity in the western Pacific (Figs. 5a,b) and is concurrent with an increase in the zonal gradient of sea surface height (SSH; Fig. 5c). This suggests that the long-term acceleration of the EUC during MAM is related to the zonal pressure gradient rather than a reduction of vertical friction. In contrast, EUC core strengthening during JJA occurs when the weakening trend in both the eastern Pacific zonal wind stress (Fig. 5a) and, to a greater extent, the westward surface current (Fig. 5b) is prominent. Therefore, it appears that

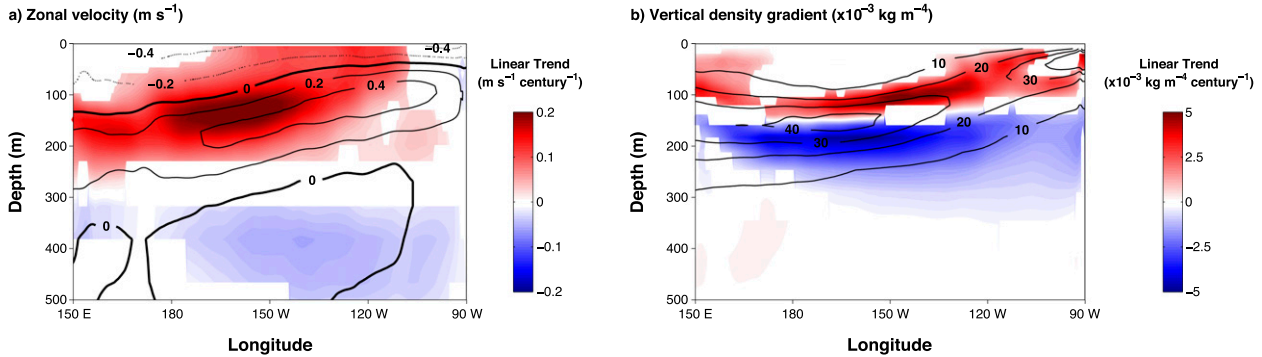


FIG. 3. Depth–lon profiles of both average and long-term trends in (a) zonal velocity and (b) density gradient along the equatorial Pacific. The solid and dashed black contours indicate the mean state of the EUC and overlying SEC in (a), respectively. Note the sign convention: positive (negative) contours indicate eastward (westward) average or trending movement. The solid black contours in (b) indicate the mean state of the vertical density gradient with positive (negative) contours indicating strengthening (weakening) stratification. Velocity and density values were averaged from 2°N to 2°S prior to calculating trends and the means state over the time span of the SODA reanalysis. Regions where the long-term trends were not significant at the 99% confidence interval were masked out.

the dynamical mechanisms driving the observed EUC intensification are caused by a seasonally dependent combination of both local (i.e., friction) and nonlocal (i.e., basin-scale pressure gradient) factors. Investigation into long-term changes in ocean kinematics from the view of the zonal momentum budget during both MAM and JJA is the subject of the following section.

b. Diagnosis of the zonal momentum equation

To formally elucidate the mechanism and drivers of historical changes in the EUC we performed a thorough analysis of the zonal momentum budget, which is similar to the approach of Brown et al. (2007) and Qiao and Weisberg (1997). We use the following rearrangement of the zonal momentum equation (ZME):

$$\frac{\partial u}{\partial t} = -u \frac{\partial u}{\partial x} - v \frac{\partial u}{\partial z} - w \frac{\partial u}{\partial z} - \frac{1}{\rho} \frac{\partial P}{\partial x} + 2\Omega v \sin\vartheta + A_H \nabla^2 u + \frac{\partial}{\partial z} \left[A_V \left(\frac{\partial u}{\partial z} \right) \right], \quad (1)$$

where $\partial u/\partial t$ is the time rate of change in zonal velocity; $u\partial u/\partial x$, $v\partial u/\partial z$, and $w\partial u/\partial z$ represent the nonlinear advective terms; $-(1/\rho)(\partial P/\partial x)$ is the zonal pressure gradient force; and $2\Omega v \sin\vartheta$ is the Coriolis force where Ω is the rotation of Earth and ϑ is the latitude at which the ZME is evaluated. Finally, $A_H \nabla^2 u$, or $(\partial/\partial x)[A_H(\partial u/\partial x)] + (\partial/\partial y)[A_H(\partial u/\partial y)]$, are the horizontal friction terms while $(\partial/\partial z)[A_V(\partial u/\partial z)]$ is the vertical friction term. All SODA fields were interpolated from their original depth divisions to regular, 5-m intervals; partial derivatives were calculated via central finite differencing. Density was calculated based on the equation of state using salinity, temperature and depth (Fofonoff and Millard 1983); A_H and A_V are the horizontal and vertical coefficients of eddy

viscosity, respectively. Because these coefficients were not retained following each model run of the SODA reanalysis (B. Giese 2013, personal communication), we estimated or calculated them in the following way: We assigned A_H a constant value of $1.5 \times 10^{-3} \text{ m}^2 \text{ s}^{-1}$ (Wallcraft et al. 2005), while we varied the value of A_V with depth: $4.5 \times 10^{-3} \text{ m}^2 \text{ s}^{-1}$ above the thermocline, $0.3 \times 10^{-3} \text{ m}^2 \text{ s}^{-1}$ within the thermocline, $1.5 \times 10^{-3} \text{ m}^2 \text{ s}^{-1}$ below the thermocline, and a smooth spline interpolation in between (Qiao and Weisberg 1997). These values are not well known and are, consequently, a primary source of uncertainty in our calculations that leads to a non-trivial mean residual. However, we only invoke the temporal change in these terms to explain seasonal EUC intensification mechanisms (i.e., Fig. 7, described in greater detail below), which is not influenced by methodological uncertainties to the same extent. Friction terms were calculated on isopycnal layers and thus all terms are displayed in an isopycnal coordinate system.

For reference, shown in Fig. 6 are the SODA record-mean longitudinal profiles of zonal wind stress τ^x and sea surface height (Fig. 6a), vertical sections of zonal velocity u (Fig. 6b), and individual terms of the zonal momentum equation (Figs. 6c–h). Note that, because of the central differencing approach used for calculating the vertical friction term, we are unable to resolve the upper and lower two isopycnal layers. The zonal pressure gradient force, nonlinear vertical advection, and vertical friction terms are the most dominant terms balancing the time-mean state and play the largest role in distinguishing the two seasonal mechanisms of EUC strengthening.

We then evaluated the change in each of the ZME components in the equatorial Pacific by differencing terms that were calculated using the seasonal, time-mean fields

for the fourth versus first quarters (i.e., each 35 yr) of the SODA reanalysis (Fig. 7). Other methods were checked to confirm the insensitivity of the salient results to such temporal choices. During MAM, the EUC strengthens at its core and in the western Pacific while a stronger surface current weakens the undercurrent and depresses the EUC core depth in the eastern Pacific (Fig. 7c). Stronger easterly trade winds coincide with stronger zonal SSH and pressure gradients (cf. Figs. 7a,g). The vertical nonlinear advective term ($w\partial u/\partial z$; Fig. 7e) exhibits a strong eastward acceleration within the upper layers of the EUC, while the vertical friction term $\{(\partial/\partial z)[A_V(\partial u/\partial z)]$; Fig. 7i} shows a westward surface acceleration, which is in opposition to the flow of the EUC.

Conversely, EUC intensification during JJA is concentrated at and near the surface of the eastern equatorial Pacific (Fig. 7d); this is zonally aligned with a pronounced weakening of the easterly trade winds (Fig. 7b) and the zonal pressure gradient force (Fig. 7h). Additionally, both the vertical nonlinear advective and friction terms (Figs. 7f,j, respectively) exhibit eastward acceleration within this region of maximum EUC strengthening (i.e., east of 160°W). EUC intensification in the west is associated with a less pronounced strengthening of the trade winds (Fig. 7b) and the zonal pressure gradient force (Fig. 7h) between 170°E and 160°W .

4. Summary and discussion

We have shown that the EUC has strengthened significantly in the SODA reanalysis since the mid-nineteenth century, a signal that is even apparent in the short-term TAO in situ record (Table 1 and Fig. 1). Analyses of long-term trends in zonal velocity indicate that this intensification entails a shoaling, vertical broadening, and westward migration of the EUC core. These structural changes in the undercurrent are tightly coupled with stratification trends and, despite different mechanisms, are similar to those projected by Luo et al. (2009; cf. Fig. 3) and Sen Gupta et al. (2012; cf. Fig. 1b).

Further investigation into equatorial Pacific climatological trends and zonal momentum budget indicates that the majority of observed, historical EUC strengthening is explained by two seasonally and dynamically different mechanisms. The intensification observed during boreal spring locally appears to be caused by a strengthening of the easterly trade winds in the west. This increases the zonal SSH gradient and, consequently, the zonal pressure gradient, which accelerates the core of the EUC in the western Pacific. The shallow, eastward acceleration in the vertical nonlinear advective term is tightly linked to this process. This advective term is influenced by intensified equatorial upwelling (i.e., larger w) because of the faster

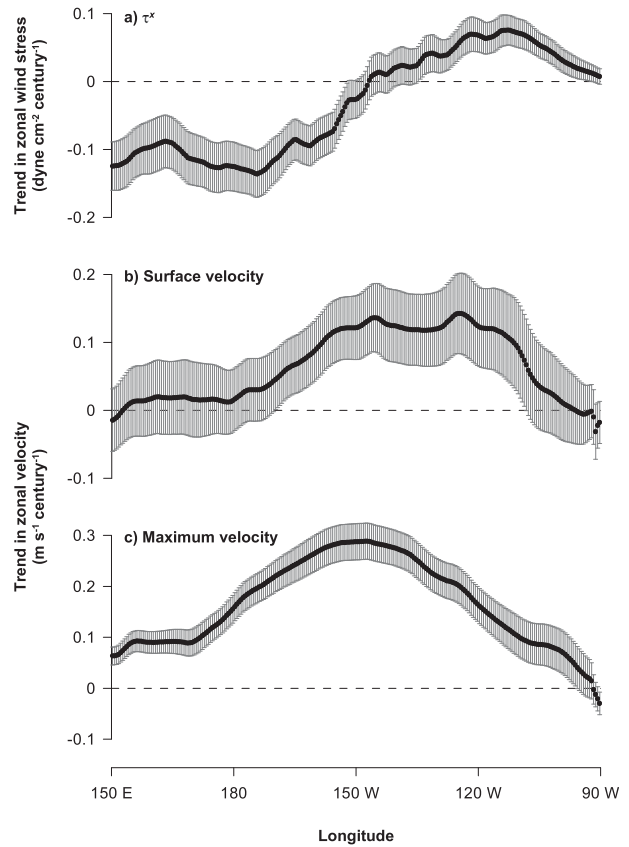


FIG. 4. Long-term trends by lon along the equator in (a) zonal wind stress and (b) surface and (c) max (i.e., EUC) zonal velocity. Error bars indicate the 99% confidence interval of the reported trend. The surface in (b) is defined as SODA's top depth layer (~ 10 m), while the EUC domain in (c) extends through SODA's first 15 subsurface depth layers (~ 10 – 300 m). Note the sign convention: positive (i.e., above the 0 line) values indicate eastward-trending movement.

westward surface current and by zonal momentum advected upward from the accelerated EUC core, which crosses a larger vertical gradient in zonal velocity (i.e., larger $\partial u/\partial z$). However, the westward wind stress, as well as subsequent vertical transmission of friction, resists this intensification and slows and depresses the core depth of the EUC in the east. This mechanism strongly resembles the mean state of the equatorial Pacific and thus operates within the canonical dynamics governing the mean EUC (e.g., Fofonoff and Montgomery 1955; Knauss 1960).

In light of historical observations of EUC weakening or even disappearance during strong El Niño events (e.g., Firing et al. 1983), it is at first counterintuitive to also observe a strengthening of the EUC during JJA when the weakening trend in both the easterly trade winds and the westward surface current is so prominent. In the SODA reanalysis, the long-term weakening of the eastern Pacific trade winds causes a local flattening of

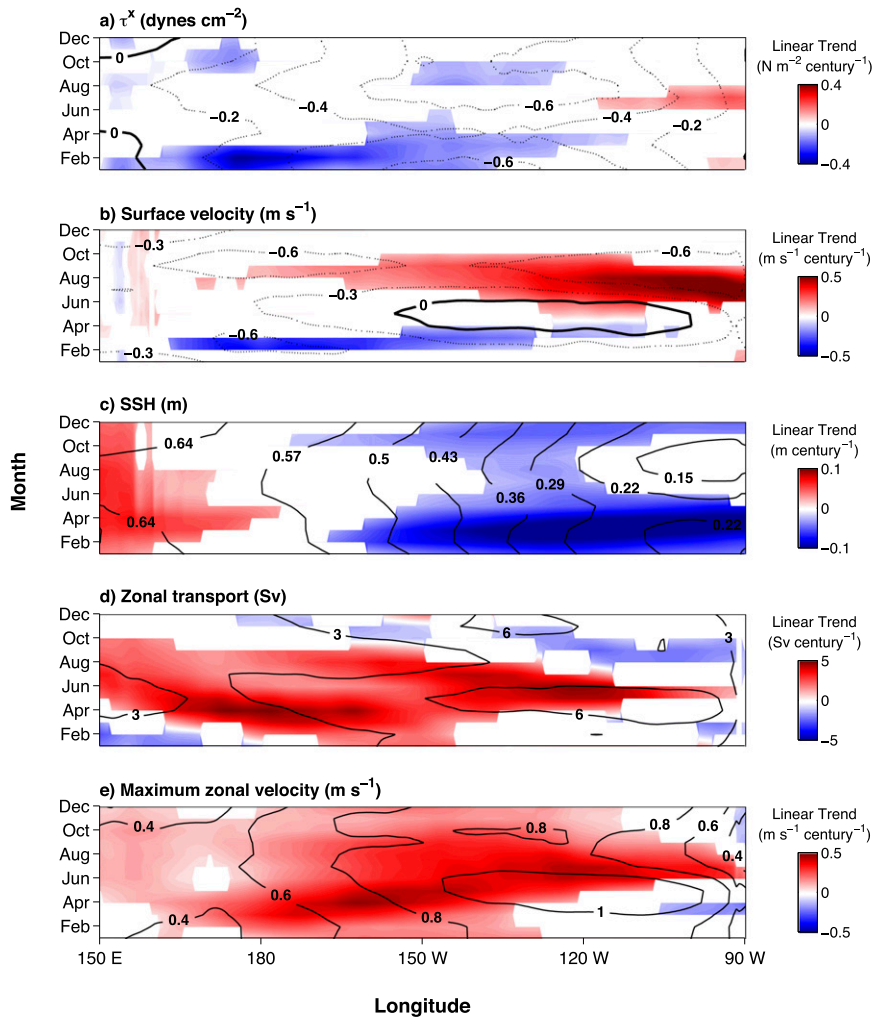


FIG. 5. Hovmöller diagrams of significant (95% confidence interval) long-term trends (filled contours) and climatologies (black contours) for (a) zonal wind stress, (b) surface velocity, (c) SSH, (d) zonal transport, and (e) max zonal (i.e., EUC) velocity on the equator. The surface in (b) is defined as the top depth layer (~ 10 m), while the transport domain in (c) extends through the top 20 depth layers in the SODA reanalysis (surface to ~ 640 m) and max velocity in (e) is evaluated between 10- and 300-m depths. Note the sign convention: positive (negative) contours indicate eastward/upward (westward/downward) average or trending movement. All long-term trends were calculated via linear regression with significance determined at the 95% confidence interval; regions where the long-term trends were not significant were masked out.

the zonal SSH and pressure gradients. If relying strictly on ENSO correlations, one might expect the EUC to weaken. Instead, we observe a strong and shallow intensification of the EUC in close synchrony with the seasonal weakening of the easterly trades. This appears to be largely apparent in the eastward acceleration in the vertical friction term $\{(\partial/\partial z)[A_V(\partial u/\partial z)]\}$, which is influenced by both the change in the vertical gradient of zonal velocity ($w\partial u/\partial z$; primarily determined here by zonal wind stress) as well as the increase in stratification (Fig. 3b). Finally, the nonlinear vertical advection term

($w\partial u/\partial z$) also contributes to shallow strengthening of the EUC. Apparently the magnitude of the change in the vertical gradient in zonal velocity ($\partial u/\partial z$) exceeds the reduction in upwelling (i.e., smaller w) that also is caused by slowing of the trades and surface current and increased stratification.

The underlying mechanism and EUC strengthening during boreal summer may be analogous to that projected by climate models, which exhibit a weakening Walker circulation (Vecchi and Soden 2007; Karnauskas and Cohen 2012). Additionally, it may be a key to

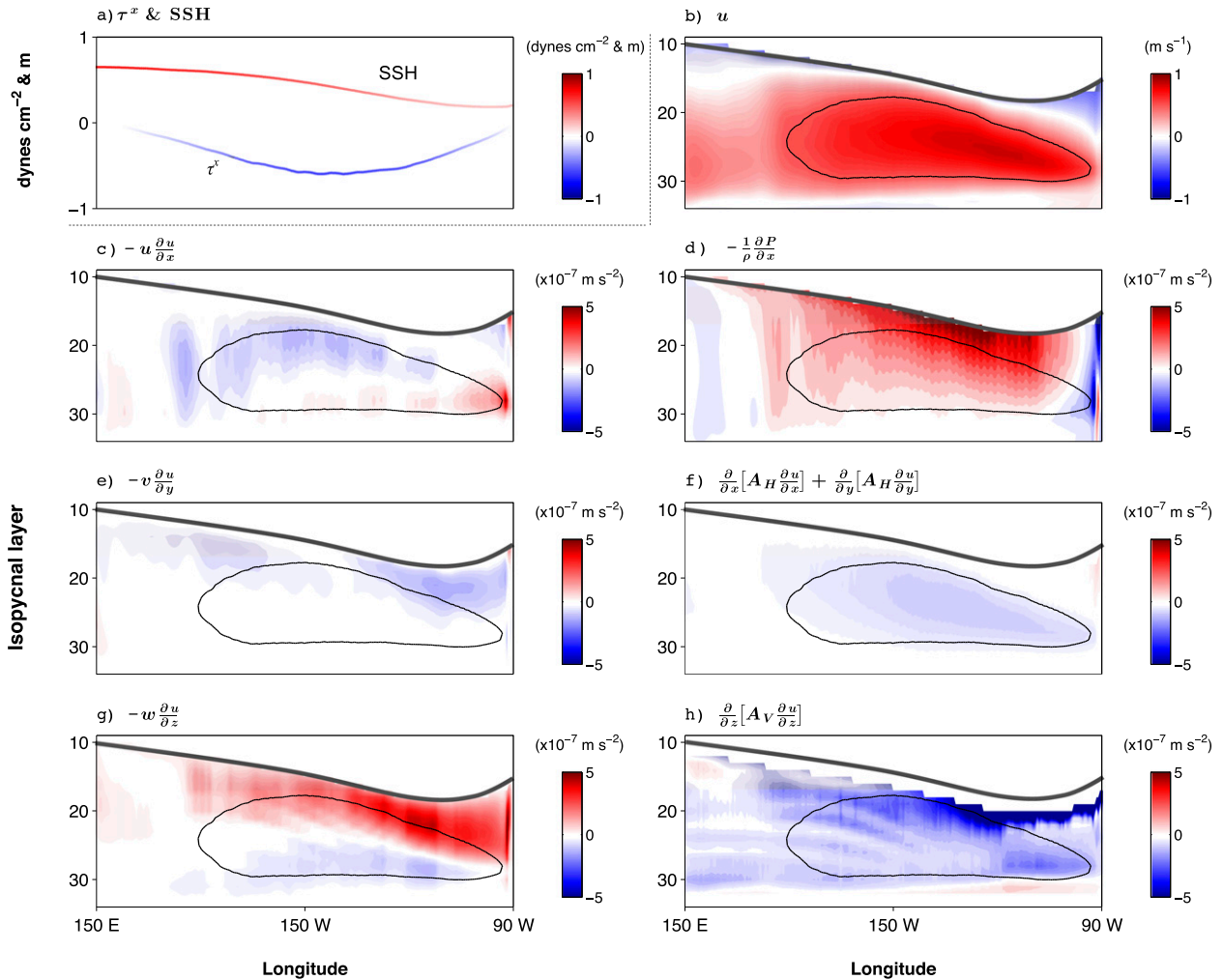


FIG. 6. Diagrams of the equatorial-mean state of (a) zonal wind stress and SSH, (b) zonal velocity, and (c)–(h) momentum budget terms. The line color in (a) reiterates the y axis and reflects the magnitude of the wind stress or SSH at a given lon. Plotting on isopycnals is given in (b)–(h) where the solid gray line indicates the surface. The solid black contours are for spatial reference and indicate the region of 0.5 m s^{-1} zonal velocity in the SODA time mean. Note the sign convention: positive (negative) contours indicate eastward (westward) movement or acceleration.

reconciling historical observations of weakened Walker circulation with strengthening Pacific zonal SST gradient. Vecchi et al. (2006) report a 3.5% slowdown of Pacific Walker circulation since 1860 (and project a 10% decrease by 2100) based on CMIP3 simulations. As they point out, such a reduction in zonal wind stress would weaken equatorial upwelling and effectively reduce the amount of cold water brought up from depth, resulting in a warming of the eastern Pacific cold tongue. However, this is fundamentally at odds with the long line of studies reporting observations of a historical cooling trend in the eastern equatorial Pacific Ocean (Cane et al. 1997; Karnauskas et al. 2009; Compo and Sardeshmukh 2010; Kumar et al. 2010; Zhang et al. 2010; Solomon and Newman 2012; L'Heureux et al. 2013). The mechanism

dominant in JJA exhibits both a weakening of the easterly trade winds, which would appear to be consistent with a weakening of the Walker circulation, and a means of increasing the zonal SST gradient: namely, a shoaling and robust strengthening of the thermocline and EUC. However, bulk measures of the Walker circulation such as SLP differences and basin-mean zonal winds, especially in an annual-mean-only basis, likely do not encapsulate the dynamics and time scales that the ocean actually responds to.

Both increased stratification and EUC intensification can be invoked as possible contributors to seasonal surface cooling. DiNezio et al. (2009) demonstrate that, despite reductions in upwelling, increased stratification (e.g., Fig. 3b) can lead to a net cooling in the eastern

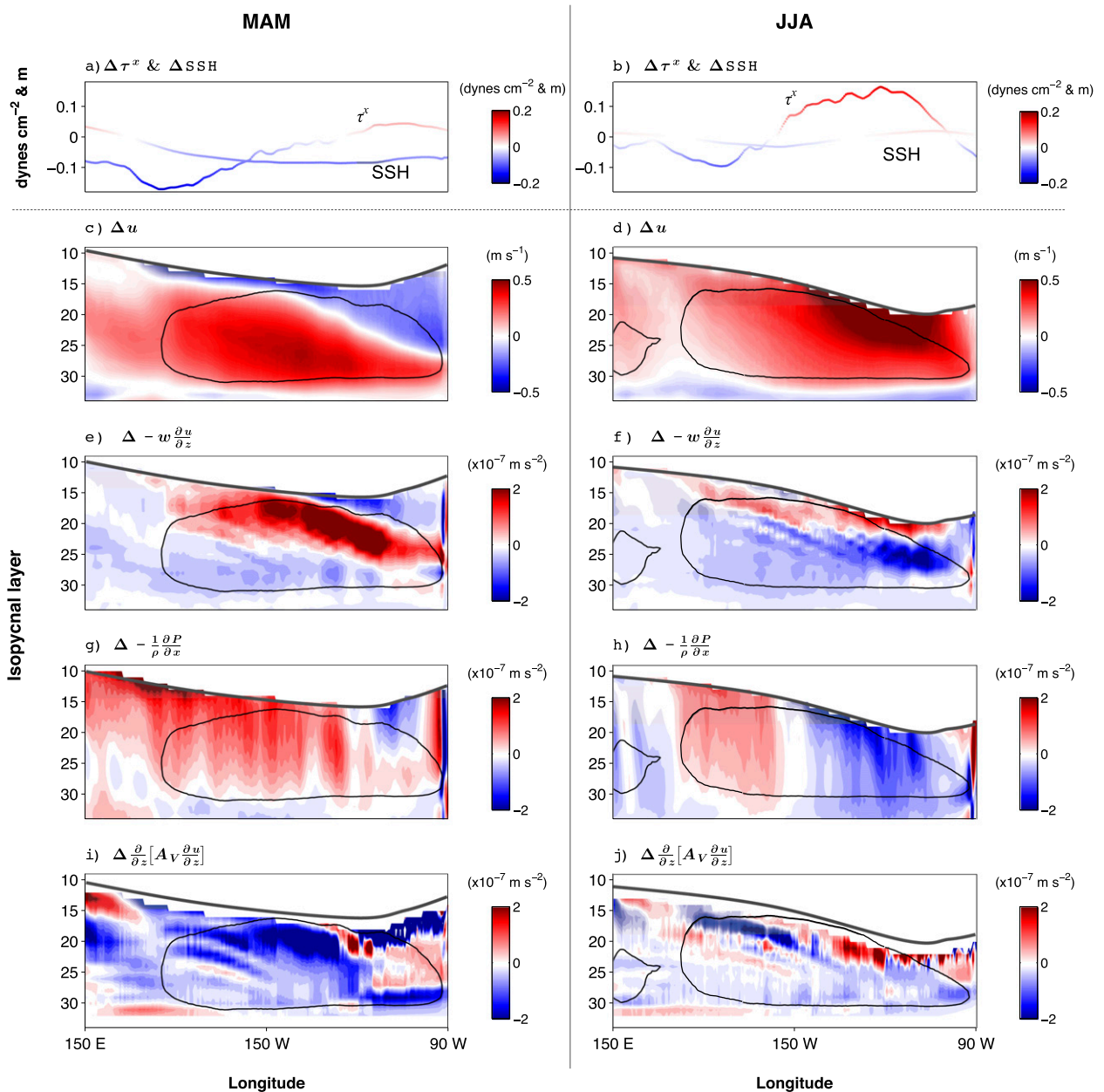


FIG. 7. Differences between the fourth and first quarters of the SODA reanalysis, by season, for (a), (b) zonal wind stress and SSH; (c), (d) zonal velocity; and (e)–(h) select momentum budget terms. The line color in (a), (b) reflects the magnitude of the wind stress or SSH at a given lon. Isopycnals are plotted in (c)–(h) where the solid gray line indicates the surface. The solid black contours spatially reference the fourth quarter, time-mean region of 0.5 m s^{-1} zonal velocity during the respective seasonal subset (i.e., MAM or JJA). Note the sign convention: positive (negative) contours indicate eastward (westward) movement or acceleration.

Pacific. Additionally, Moum et al. (2013) highlight the critical role of ocean mixing driving sea surface cooling during boreal summer. Changing subsurface zonal velocity and vertical shear may further stimulate turbulent mixing and enhance this seasonal cooling. Certainly the efficacy of the coupling mechanism we propose here depends upon a number of factors: not least of which is

the impact of climate change on the temperature of the water masses that feed the EUC (Cane et al. 1997). Further work focusing on the mixed-layer heat budget is necessary to confirm this speculation but may yield a mechanism parallel to that described by Sun and Liu (1996), Clement et al. (1996), and Seager and Murtugudde (1997) as an ocean dynamical thermostat.

It should be noted that this study does not directly address off-equatorial mechanisms for EUC trends, and recent studies such as those addressing the western boundary currents that feed the EUC as prominent drivers of intensification (Luo et al. 2009; Sen Gupta et al. 2012) are possibly complementary rather than mutually exclusive. Indeed, our momentum budget analyses focus on the two seasons that exhibit the largest increase in maximum zonal velocity and transport. However, these fields, particularly maximum velocity (Fig. 5e), show strengthening throughout most of the annual cycle. This may be driven by an increase in the zonal sea surface height gradient (and thus, pressure gradient force), which is characterized in part by a persistent, year-long elevation in the western Pacific (Fig. 3c). This signal is highly suggestive of off-equatorial drivers such as strengthening western boundary currents, for both their dynamical influence and the absence of a clear causative signal in seasonal wind stress (Fig. 5a), and further illustrates the potential for multiple oceanic–atmospheric drivers contributing to changing tropical circulation.

A strengthening of the EUC has important implications for affected equatorial Pacific island and oceanic ecosystems. Topographic upwelling of the EUC delivers cold, nutrient- and CO₂-rich water to the surface and plays a fundamental role in dictating the structure and evolution of exposed ecosystems (Houvenaghel 1978). Such regions have been proposed as potential priorities for enhanced conservation efforts because they may locally mitigate and are thus resilient to the rapidity of ocean surface warming that poses a serious threat to tropical coral reef ecosystems (West and Salm 2003). Karnauskas and Cohen (2012) specifically highlight the refugia potential of equatorial Pacific islands because of the modeled cooling influence of predicted EUC intensification. However, enhanced upwelling could also adversely impact exposed coral reefs because CO₂-rich EUC water may deter calcium carbonate and thus essential framework production on these ecosystems (Feely et al. 2008; Manzello et al. 2008). An historical precedence for EUC intensification is valuable because investigation into past reef response to EUC strengthening may enable fishery managers and marine conservation planners to better anticipate and plan for the inevitable ecological consequences of future changes in ocean temperatures, circulation, and nutrient supply.

Acknowledgments. The authors gratefully acknowledge Benjamin Giese for his tireless efforts to improve the SODA reanalysis product, for his assistance in procuring the version 2.2.6 fields, and for his insightful feedback on this manuscript. The authors also thank the

three anonymous reviewers for their constructive suggestions. EJD is supported by NSF Grants OCE-1031971 and OCE-1233282. KBK is supported by NSF Grant OCE-1233282.

REFERENCES

- Arthur, R. S., 1960: A review of the calculation of ocean currents at the equator. *Deep-Sea Res.*, **6**, 287–297.
- Bjerknes, J., 1966: A possible response of the atmospheric Hadley circulation to equatorial anomalies of ocean temperature. *Tellus*, **18**, 820–829.
- , 1969: Atmospheric teleconnections from the equatorial Pacific. *Mon. Wea. Rev.*, **97**, 163–172.
- Brown, J. N., J. S. Godfrey, and R. Fiedler, 2007: A zonal momentum balance on density layers for the central and eastern equatorial Pacific. *J. Phys. Oceanogr.*, **37**, 1939–1955.
- Cane, M. A., A. C. Clement, A. Kaplan, Y. Kushnir, D. Pozdnyakov, R. Seager, S. E. Zebiak, and R. Murtugudde, 1997: Twentieth-century sea surface temperature trends. *Science*, **275**, 957–960.
- Carton, J. A., and B. S. Giese, 2008: A reanalysis of ocean climate using Simple Ocean Data Assimilation (SODA). *Mon. Wea. Rev.*, **136**, 2999–3017.
- Clement, A., R. Seager, M. A. Cane, and S. E. Zebiak, 1996: An ocean dynamical thermostat. *J. Climate*, **9**, 2190–2196.
- Compo, G. P., and P. D. Sardeshmukh, 2010: Removing ENSO-related variations in the climate record. *J. Climate*, **23**, 1957–1978.
- , and Coauthors, 2011: The Twentieth Century Reanalysis Project. *Quart. J. Roy. Meteor. Soc.*, **137**, 1–28.
- DiNezio, P. N., A. C. Clement, G. A. Vecchi, B. J. Soden, B. P. Kirtman, and S.-K. Lee, 2009: Climate response of the equatorial Pacific to global warming. *J. Climate*, **22**, 4873–4892.
- Feely, R. A., T. Takahashi, R. Wanninkhof, M. J. McPhaden, C. E. Cosca, S. C. Sutherland, and M.-E. Carr, 2006: Decadal variability of the air–sea CO₂ fluxes in the equatorial Pacific Ocean. *J. Geophys. Res.*, **111**, C08S90, doi:10.1029/2005JC003129.
- , C. L. Sabine, J. M. Hernandez-Ayon, D. Ianson, and B. Hales, 2008: Evidence for upwelling of corrosive ‘acidified’ water onto the continental shelf. *Science*, **320**, 1490–1492.
- Firing, E., R. Lukas, J. Sadler, and K. Wyrtki, 1983: Equatorial undercurrent disappears during 1982–1983 El Niño. *Science*, **222**, 1121–1123.
- Fofonoff, N. P., and R. B. Montgomery, 1955: The equatorial undercurrent in the light of the vorticity equation. *Tellus*, **7**, 518–521.
- , and R. C. Millard, 1983: Algorithms for computation of fundamental properties of seawater. UNESCO Tech. Paper in Marine Science 44, 53 pp.
- Ganachaud, A., A. Sen Gupta, J. N. Brown, K. Evans, C. Maes, L. C. Muir, and F. S. Graham, 2012: Projected changes in the tropical Pacific Ocean of importance to tuna fisheries. *Climatic Change*, **119**, 163–179.
- Gove, J. M., M. A. Merrifield, and R. E. Brainard, 2006: Temporal variability of current-driven upwelling at Jarvis Island. *J. Geophys. Res.*, **111**, C12011, doi:10.1029/2005JC003161.
- Houvenaghel, G. T., 1978: Oceanographic conditions in the Galapagos Archipelago and their relationships with life on the islands. *Upwelling Ecosystems*, R. Boje and M. Tomczak, Eds., Springer, 181–200.
- Johnson, G. C., B. M. Sloyan, W. S. Kessler, and K. E. McTaggart, 2002: Direct measurements of upper ocean currents and water

- properties across the tropical Pacific during the 1990s. *Prog. Oceanogr.*, **52**, 31–61.
- Julian, P. R., and R. M. Chervin, 1978: A study of the Southern Oscillation and Walker circulation phenomenon. *Mon. Wea. Rev.*, **106**, 1433–1451.
- Karnauskas, K. B., and A. L. Cohen, 2012: Equatorial refuge amid tropical warming. *Nat. Climate Change*, **2**, 530–534.
- , R. Seager, A. Kaplan, Y. Kushnir, and M. A. Cane, 2009: Observed strengthening of the zonal sea surface temperature gradient across the equatorial Pacific Ocean. *J. Climate*, **22**, 4316–4321.
- , G. C. Johnson, and R. Murtugudde, 2012: An equatorial ocean bottleneck in global climate models. *J. Climate*, **25**, 343–349.
- Keeling, C. D., R. B. Bacastow, A. E. Bainbridge, C. A. Ekdahl, P. R. Guenther, L. S. Waterman, and J. F. S. Chin, 1976: Atmospheric carbon-dioxide variations at Mauna-Loa Observatory, Hawaii. *Tellus*, **28**, 538–551.
- Knauss, J. A., 1960: Measurements of the Cromwell Current. *Deep-Sea Res.*, **6**, 265–274.
- , 1966: Further measurements and observations on the Cromwell Current. *J. Mar. Res.*, **24**, 205–239.
- Kumar, A., B. Jha, and M. L'Heureux, 2010: Are tropical SST trends changing the global teleconnection during La Niña? *Geophys. Res. Lett.*, **37**, L12702, doi:10.1029/2010GL043394.
- L'Heureux, M. L., S. Lee, and B. Lyon, 2013: Recent multidecadal strengthening of the Walker circulation across the tropical Pacific. *Nat. Climate Change*, **3**, 571–576.
- Luo, Y., L. M. Rothstein, and R.-H. Zhang, 2009: Response of the Pacific subtropical-thermocline water pathways and transports to global warming. *Geophys. Res. Lett.*, **36**, L04601, doi:10.1029/2008GL036705.
- Mann, M. E., R. S. Bradley, and M. K. Hughes, 1999: Northern hemisphere temperatures during the past millennium: Interferences, uncertainties, and limitations. *Geophys. Res. Lett.*, **26**, 759–762.
- Manzello, D. P., J. A. Kleypas, D. A. Budd, C. M. Eakin, P. W. Glynn, and C. Langdon, 2008: Poorly cemented coral reefs of the eastern tropical Pacific: Possible insights into reef development in a high-CO₂ world. *Proc. Natl. Acad. Sci. USA*, **105**, 10450–10455.
- McPhaden, M. J., and B. A. Taft, 1988: Dynamics of seasonal and interannual variability in the eastern equatorial Pacific. *Phys. Oceanogr.*, **18**, 1713–1732.
- , and Coauthors, 1998: The Tropical Ocean-Global Atmosphere observing system: A decade of progress. *J. Geophys. Res.*, **103**, 14169–14240.
- Moum, J. N., A. Perlin, J. D. Nash, and M. J. McPhaden, 2013: Seasonal sea surface cooling in the equatorial Pacific cold tongue controlled by ocean mixing. *Nature*, **500**, 64–67.
- Philander, S. G. H., 1973: Equatorial undercurrent: Measurements and theories. *Rev. Geophys.*, **11**, 513–570.
- , W. J. Hurlin, and A. D. Seigel, 1987: Simulation of the seasonal cycle of tropical Pacific Ocean. *J. Phys. Oceanogr.*, **17**, 1986–2002.
- Qiao, L., and R. H. Weisberg, 1997: The zonal momentum balance of the equatorial undercurrent in the central Pacific. *J. Phys. Oceanogr.*, **27**, 1094–1119.
- Seager, R., and R. Murtugudde, 1997: Ocean dynamics, thermocline adjustment, and regulation of tropical SST. *J. Climate*, **10**, 521–534.
- Seidel, H. F., and B. Giese, 1999: Equatorial currents in the Pacific Ocean 1992–1997. *J. Geophys. Res.*, **104**, 7849–7863, doi:10.1029/1999JC900036.
- Sen Gupta, A., A. Ganachaud, S. McGregor, J. N. Brown, and L. Muir, 2012: Drivers of the projected changes to the Pacific Ocean equatorial circulation. *Geophys. Res. Lett.*, **39**, L09605, doi:10.1029/2012GL051447.
- Solomon, A., and M. Newman, 2012: Reconciling disparate twentieth-century Indo-Pacific ocean temperature trends in the instrumental record. *Nat. Climate Change*, **2**, 691–699.
- Sun, D.-Z., and Z. Liu, 1996: Dynamic ocean-atmosphere coupling: A thermostat for the tropics. *Science*, **272**, 1148–1150.
- Vecchi, G. A., and B. J. Soden, 2007: Global warming and the weakening of the tropical circulation. *J. Climate*, **20**, 4316–4340.
- , A. T. Wittenberg, I. M. Held, A. Leetmaa, and M. J. Harrison, 2006: Weakening of tropical Pacific atmospheric circulation due to anthropogenic forcing. *Nature*, **441**, 73–76.
- Wallcraft, A. J., A. B. Kara, and H. E. Hurlburt, 2005: Convergence of Laplacian diffusion versus resolution of an ocean model. *Geophys. Res. Lett.*, **32**, L07604, doi:10.1029/2005GL022514.
- West, J. M., and R. V. Salm, 2003: Resistance and resilience to coral bleaching: Implications for coral reef conservation and management. *Conserv. Biol.*, **17**, 956–967.
- Wyrtki, K., and B. Kilonsky, 1984: Mean water and current structure during the Hawaii-to-Tahiti shuttle experiment. *J. Phys. Oceanogr.*, **14**, 242–254.
- Yang, C., and B. S. Giese, 2013: El Niño Southern Oscillation in an ensemble ocean reanalysis and coupled climate models. *J. Geophys. Res. Oceans*, **118**, 4052–4071, doi:10.1002/jgrc.20284.
- Zhang, W., J. Li, and X. Zhao, 2010: Sea surface temperature cooling mode in the Pacific cold tongue. *J. Geophys. Res.*, **115**, C12042, doi:10.1029/2010JC006501.